THE JOURNAL OF PHYSICAL CHEMISTRY C

Article

pubs.acs.org/JPCC

How Ion Condensation Occurs at a Charged Surface: A Molecular Dynamics Investigation of the Stern Layer for Water−Silica Interfaces

Sarah Hocine,[†] Remco Hartkamp,[‡,§,∥] Bertrand Siboulet,[*,⊥] Magali Duvail,[⊥] Benoit Coasne,[‡,§,∥] Pierre Turq,[#] and Jean-François Dufrêche[*,⊥]

[†]Institut de Chimie Séparative de Marcoule ICSM, UMR 5257 CEA - CNRS - ENSCM - Université Montpellier, Bâtiment 426, F-30207 Bagnols-sur-Cèze, France

[‡]MultiScale Material Science for Energy and Environment, CNRS/MIT (UMI 3466), 77 Massachussetts Avenue, Cambridge, Massachusetts 02139, United States

[§]Institut Charles Gerhardt Montpellier, ENSCM, Université Montpellier 2 and CNRS (UMR 5253), 8 rue Ecole Normale, 34296 Montpellier, France

[∥]Department of Civil and Environmental Engineering, Massachusetts Institute of Technology, 77 Massachusetts Avenue, Cambridge, Massachusetts 02139, United States

[⊥]Institut de Chimie Séparative de Marcoule ICSM, UMR 5257 CEA - CNRS - ENSCM - Université Montpellier 2, Bâtiment 426, F-30207 Bagnols-sur-Cèze, France

[#]Université Pierre et Marie Curie Paris VI, UMR 8234, PHENIX, F-75005 Paris, France

ABSTRACT: We investigate the Stern layer of charged silica−water interfaces by calculating the ion−surface interaction from molecular dynamics simulations. The McMillan−Mayer potentials of mean force between a charged oxygen site and a lithium or cesium cation have been calculated. Contact ion pairs (CIPs) are important for the adsorption and desorption of ions, especially for lithium. An activation energy appears, which can result in a large estimated relaxation time. In the case of lithium, time scales needed to bind or unbind ions to and from the surface are found to be very long (up to the order of seconds for some surfaces), which implies that molecular dynamics cannot always be fully equilibrated. This work provides a new image of the Stern layer: it is not a continuous layer but a set of Bjerrum pairs. As a matter of fact, quantitative (macroscopic) treatments of such systems with localized surface charges require a three-dimensional model, contrary to the more commonly used one- or two-dimensional theoretical treatments.

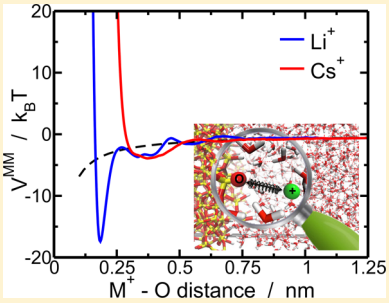

1. INTRODUCTION

Charged nanoporous materials attract considerable attention because of their use in numerous applications: water purification, ion retention, drug delivery, sensors, and energy storage, among others. Within this context, the description of the electrical double layer (EDL), which represents the charge distribution in the vicinity of a charged surface in water, is very important.[1] Since the pioneering approach by Gouy and Chapman, based on the Poisson−Boltzmann equation, many improvements have been proposed. It is now widely accepted that far away from the interface charges are distributed along a diffusive layer, which can be modeled by continuum models (such as the original Gouy−Chapman approach).[1] However, at contact with the interface, the molecular nature of the constituents (solvent and ions) becomes predominant, and a specific treatment is needed, deviating from the Gouy−Chapman approach. Numerous works have been devoted to studying the first layer of condensed ions, which can be adsorbed on the surface.[2,3] Such adsorbed ions are typically described with the concept of the Stern layer.

When looking at the charge of solid surfaces, a distinction can be made between the two following situations. On the one hand, for some systems, the charge can be modeled as a volume charge that comes from an excess of cations or anions. For these systems, such as clays,[4−6] continuum theories such as the Gouy−Chapman equation are suitable when compared to molecular simulations or experiments. On the other hand, for many other solids, including metal oxides such as silica, the charge arises from the hydrolysis of the metal atom to M−OH and the consequent binding or dissolution of H^+ ions. In this case, the charge is highly localized at surface sites, and the corresponding Stern layer[2,3] requires a specific treatment since continuum theories are no longer valid. The system is then commonly modeled using effective parameters (zeta potential, effective charge) that account for the complex ion/surface interactions. Such a task is even more difficult to achieve as the ion distributions can be very different in the case of a homogeneously charged surface from the case of a locally charged surface.[7,8]

Received: September 10, 2015
Revised: November 18, 2015
Published: December 14, 2015

DOI: 10.1021/acs.jpcc.5b08836
J. Phys. Chem. C 2016, 120, 963−973

Among the materials falling in the second category above, silica is probably the most studied because of its ubiquitous nature.[9−15] Silica−water interfaces can be neutral or charged, depending on the composition of the water, especially the pH, which controls the ionization of the silanol groups. The average surface charge, as well as the charge distribution, are important parameters in the description of such systems. In this article, we study charged silica−water interfaces in order to understand how the specifics of the Stern layer depend on the adsorption energies and binding times of ions at charged sites. When charges result from substitution of charged atoms inside the solid, e.g., for clays, the electrostatic interactions with solvated ions are small due to a large minimum approach distance between the ions and the charged sites; i.e., the solvated ions cannot penetrate into the solid. On the other hand, when a surface charge results from the presence of small charged atoms in direct contact with the electrolyte solution, such as the functional groups at the silica surface, the local electrostatic field is very strong, and the adsorption phenomenon is difficult to model. In this work, we study situations in which the localized charge leads to strong electrostatic interactions. One of our main purposes is to use molecular dynamics simulations to study how to include these strong interactions in a comprehensive model.

A surface bears a net charge that arises from the balance between protonation and deprotonation of the surface. If we consider an oxide surface (such as amorphous silica) having a silanol density up to 5 nm^{-2},[16] a fully deprotonated surface (which would occur at high pH) would result in a surface charge density of −0.8 C m^{-2}. However, at near-neutral pH, partial deprotonation tends to occur to an extent that also depends on other environmental conditions. Titration experiments give the amount of protons exchanged with cations in the solution. Typical values resulting from such an exchange are around −0.15 to −0.10 C m^{-2}.[17] Contrary to the assumption of the Gouy−Chapman approximation, the effective charge depends not only on the charge of the ions but also on their discrete nature.

Most of the numerous works on molecular modeling of silica have been devoted to neutral silica. For these systems, the silanol density allows the surface hydrophilicity to be controlled.[18,19] The distributions and the dynamics of the surrounding water molecules depend on the surface roughness. Nevertheless, the domain in which the solvent molecules are directly perturbed by the surface is relatively small; the density near an interface typically shows two inhomogeneous layers beyond which bulk equilibrium and transport properties are recovered.[20] Despite its significance for the applications mentioned above, the case of charged silica has received much less attention from a molecular simulation point of view. Care must be taken in how charge surface groups are modeled since this can greatly affect the electric double layer. Upon deprotonation of a silanol, the net local charge of the oxygen is $-1e$ (e being the elementary charge), but this value does not directly give the charge used in molecular simulations. This net local charge can be distributed among surrounding atoms, as has been done in some studies.[21,22] In contrast, some authors have validated a model in which deprotonated silanol groups do not carry a $-1e$ local charge.[23] Considering the importance of charge repartition and the variety of the total charges in published results, we propose here a comparison between two charges for deprotonated silanol, namely, setting the charge to −1 or $-1.5e$ on the deprotonated oxygen.

Many recent molecular dynamics simulation studies of electrokinetic phenomena near charged silica−water interfaces have shown that ions are largely immobile close to the interface, where the water streaming velocity goes to zero.[7,22,24,25] The macroscopic Navier−Stokes equation appears to be valid at a nanometer range, but the electrokinetic streaming velocity becomes strongly dependent on the fitted boundary conditions. Indeed, the external force on the fluid is proportional to the charge density of the *mobile* charges, while the immobile ions do not contribute to the streaming motion. Consequently, an accurate description of the counterion layer, including a robust description of the ion−surface interactions, is required in order to predict electrokinetic phenomena.

In this paper, we describe the Stern layer by calculating the potential of mean force (PMF) between a charged O^- site at the silica surface and a counterion (Li^+ or Cs^+) solvated in water. The potential of mean force is of fundamental significance in order to describe the molecular nature of the Stern layer because many equilibrium quantities (effective charges, ionic exchange, mass action law constants (K_d), etc.) can be deduced from it by using the McMillan−Mayer formalism.[26,27] This approach generalizes recent works on pairing in bulk electrolytes[28−31] of ions at a solid interface. The concept of Bjerrum association represents a cation−anion pair that forms an electrostatic stable association or a contact ion pair (CIP). An electrostatic stable association can in fact be a CIP or a solvent-separated ion pair (SSIP). Both are referred to as a Bjerrum pair, which behaves as if it is a single neutral species in the solution. When ions are small or highly charged, cations and anions can form pairs that are stable for long times (depending on the nature of the ions).[32] The formation of strong ion pairs between counterions and charged surface oxygens could impair the possibility to reach equilibrium at short times in molecular simulation. Determination of the McMillan−Mayer potential, as done in this paper, provides quantitative insights into this question.

The remainder of this paper is organized as follows. In Section 2, we introduce the details of the molecular dynamics simulations and describe the method used for calculating the potential of mean force between an ion and a charged surface. Section 3 presents our results as a function of the number of charged sites at the surface and the nature of the counterion. The calculated McMillan−Mayer potential of mean force is used in a simple density functional theory (DFT) in order to calculate the ion distribution profile at equilibrium. Finally, association constants and average binding and unbinding times are estimated from a simple approach based on the Fokker−Planck equation.

2. METHODS

2.1. Molecular Dynamics for Umbrella Sampling. We perform PMF calculations using molecular dynamics (MD) combined with the umbrella sampling technique (US). We consider the interactions between a solvated cation and a deprotonated silanol group at the silica surface. The MD simulations are performed in a periodic simulation box with dimensions 2.852 nm for x and y and 5.0 nm for z (z is the direction normal to the silica surface). The width of the channel is approximately 4.0 nm (Figure 1).

The interaction energy is given by the sum of short-range (nonelectrostatic) repulsive interactions and Coulombic (electrostatic) interactions. The short-range interactions are modeled through the Lennard-Jones (eq 1) potential and the

DOI: 10.1021/acs.jpcc.5b08836
J. Phys. Chem. C 2016, 120, 963−973

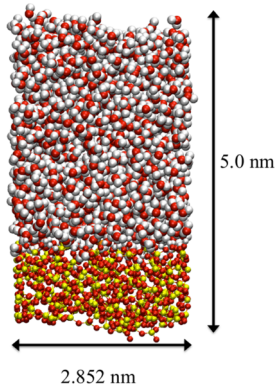

Figure 1. Side view of the periodic simulation box. For the substrate, the oxygen and silicon atoms are shown in red and yellow. The hydrogen and oxygen atoms of water in the channel are the white and red spheres.

PN-TrAZ potential.[33,34] The latter is implemented through the "nm" Lennard-Jones formula (eq 2).

$$U_{LJ}(r_{jk}) = 4\epsilon_{jk}\left(\left(\frac{\sigma}{r_{jk}}\right)^{12} - \left(\frac{\sigma}{r_{jk}}\right)^{6}\right) \quad (1)$$

$$U_{nm}(r_{jk}) = \frac{E_0}{n-m}\left(m\left(\frac{r_0}{r_{jk}}\right)^{n} - n\left(\frac{r_0}{r_{jk}}\right)^{m}\right) \quad (2)$$

The parameters used for the short-range interaction potentials are given in Table 1.

We used three surfaces of varying hydrophilicity which are modified versions of previously published surfaces.[19] The most hydrophobic surface is completely deprotonated, while the two hydrophilic surfaces are generated by adding silanols and relaxing the surfaces using molecular dynamics. An important issue for these surfaces is that in all siloxane bridges, namely Si−O−Si, distances are very close to 0.16 nm. This distance is the bulk value for silica, but we obtained it also for all surface siloxanes. If the siloxane distances were too long, it would increase the hydrophilicity. Water molecules, which are modeled via the rigid three-point SPC/E model,[35] are then added in the channel. The temperature of the fluid is controlled using a Berendsen thermostat[36] with the target temperature of 300 K and a coupling time of 0.5 ps. The pressure is controlled implicitly by fine-tuning the number of water molecules so that the water density in the center of the box is very close to the bulk density of SPC/E water. We reach a density of 33.428 water molecules per cubic nanometer, which is slightly above but very close to (+0.5%) the SPC/E density at 1 atm.[37]

Table 1. Short-Range Pair Interaction Potentials Used in the Molecular Dynamics Simulations[a]

		E_0	n	m	r_0	refs
O_w	Si	0.07290	15.49670	6.58589	4.33870	33
O_w	O_s	0.65819	11.61320	7.28875	3.70378	33
O_w	H_s	0.39202	7.85993	7.85989	2.92660	33
H_w	Si	0.03507	13.27250	6.71192	3.81270	33
H_w	O_s	0.47530	8.25792	8.25791	3.02920	33
H_w	H_s	0.48864	6.32666	6.32705	2.09800	33
		ϵ_{jk}	σ_{jk}			
O_w	O_c	0.65000	3.1660			35
O_w	O_w	0.65000	3.1660			35
O_w	Cs	0.52160	3.5265			42
Cs	Cs	0.41800	3.8840			35, 42
Cs	O_c	0.52050	3.5190			42, 43
Cs	O_s	0.52050	3.5190			42, 43
Cs	Si	0.47230	3.8395			42, 43
O_w	Li	0.67000	2.3376			42, 44
Li	Li	0.69082	1.5060			35, 42
Li	O_c	0.66940	2.3300			43, 44
Li	O_s	0.66940	2.3300			43, 44
Li	Si	0.60710	2.6505			43, 44

[a]The PN-TrAZ potential[34] for water−surface interaction was fitted against an "*nm*" potential.[33] All other interaction potentials are Lennard-Jones potentials with the cross terms obtained using the Lorentz−Berthelot mixing rules. Energies are in kJ mol^{-1}, and distances are in Å.

The silica is kept frozen in the course of the simulations. The surfaces exhibit 1, 29, and 57 silanols to vary the hydrophilicity (Figure 2). A single deprotonated silanol site is given a net charge of $-1e$ where e is the elementary charge. Given the dimensions of the silica surface (2.852^2 nm^2), this charge site causes the surface to have a charge density of −0.02 C m^{-2} (or 0.12 e nm^{-2}). This is below the typical charge densities found for silica surfaces with monovalent counterions.[17] We compare the interaction with the surface for two cation species: lithium (Li^+) and cesium (Cs^+). These ions correspond to the lower and upper ends of the alkali series, respectively. The PMF calculations described below are between one of these two ions and a charged surface oxygen atom, representing a deprotonated silanol.

The electrostatic interaction between an ion and the surface depends in part on the charge of the deprotonated silanol. Determining how much charge should be assigned to the deprotonated oxygen atom is an open question. Indeed, some authors use charge values in which the net charge of a deprotonated silanol is not $-1.0e$.[23] This subtle point has important consequences on physical quantities such as association constants, ion distribution, and eventually electrokinetics. For this reason, we perform a parametric study for the net charge on the dangling oxygen (−1.5 or $-1e$), aiming at determining upper and lower boundaries for association constants and dynamics. The two sets (C1 and C2) of charges on silica atoms are given in Table 2.

All molecular dynamics simulations are performed with DL_POLY[38] using Verlet's algorithm with a simulation time step of 1 fs. The simulations are equilibrated for 1 ns followed by a production run of 2 ns. Analysis was processed using WHAM (Weighted Histogram Analysis Method) Version 2.0.9,[39] Mathematica 8,[40] and VMD.[41]

2.2. Potential of Mean Force via Umbrella Sampling.

The PMF between a substrate site and a free ion is a McMillan−Mayer potential which corresponds to the potential for a solute in a continuous medium. The latter can be calculated using the Umbrella Sampling (US) procedure[45−47] which produces the excess free energy as a function of one or more variables (in our case the distance to the silica surface). The US technique consists of imposing a harmonic potential to constrain the movement of the ion, in order to allow sampling states of the phase space that are energetically unfavorable. Sampling is performed with the harmonic spring connected to various locations (windows) to cover different distances to the interface. Window spacing and stiffness are adjusted iteratively such that the resulting series of sampled data covers the whole

DOI: 10.1021/acs.jpcc.5b08836
J. Phys. Chem. C 2016, 120, 963−973

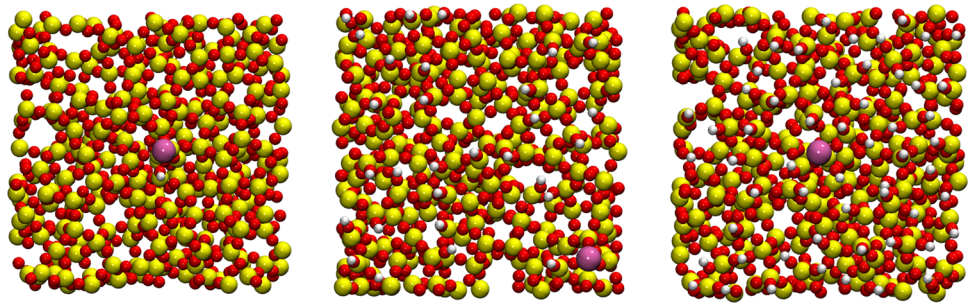

Figure 2. Surface hydrophilicity is controlled through the silanol density: (from left to right) 1, 29, and 57 silanols on 2.852^2 nm^2. For each surface, one silanol is deprotonated with the single O_c shown in mauve, and the position of the solvated lithium or cesium (not shown) is monitored. Other oxygen atoms are red, while hydrogen and silicon atoms are the white and yellow spheres, respectively.

Table 2. Charge Sets Used in the Present Work[a]

potentials	H_s	O_s	Si	O_c
C1	0.5	−1	2	−1.5
C2	0.5	−1	2	−1

[a]Values are in units of elementary charge e. H_s silanol hydrogen, O_s bulk oxygen, Si bulk silicon, and O_c dangling oxygen. See Figure 3.

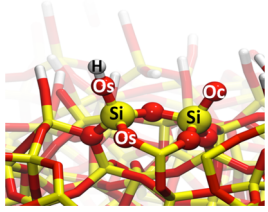

Figure 3. Visualization of the protonated and deprotonated surface groups.

range of distances with a sufficient overlap between adjacent umbrellas. The spring stiffness ranges from 20 to 1000 kJ mol^{-1} Å^{-2}. The sampling in each window provides biased simulation data that can be combined into an unbiased potential of mean force using the Weighted Histogram Analysis Method (WHAM).[39]

We simulate a situation in which an ion is located on top of a deprotonated oxygen site and moves only in the direction normal to the surface. Movement in the perpendicular directions is suppressed by a stiff harmonic potential imposed on the angle between the vector normal to the silica surface and the vector between the ion and the oxygen (see Figure 8). We checked thoroughly that the angle constraint does not impact the PMF profile, as will be demonstrated below. When US is performed between two ions in a bulk solution, the resulting potential $V^{US}(r)$ versus distance r has to be corrected for an entropic term to yield the McMillan−Mayer potential $V^{MM}(r)$

$$V^{MM}(r) = V^{US}(r) + 2k_BT \ln(r) \tag{3}$$

where k_B is Boltzmann's constant and T the temperature. This correction is needed because $V^{US}(r)$ is defined as the density probability as a function of r (scalar variable), whereas $V^{MM}(r)$ is defined as the density probability as a function of $\mathbf{r}$ (vector variable). Thus, an elementary volume $4\pi r^2$ has to be taken into account when relating the density of states $\mathcal{P}(r)$ (reconstructed from the US technique) to the McMillan-Mayer potential of mean force

$$\mathcal{P}(r)\mathrm{d}r = \alpha_1 \exp(-\beta V^{US}(r))\mathrm{d}r = \alpha_2 \exp(-\beta V^{MM}(r))4\pi r^2 \mathrm{d}r \tag{4}$$

where $\beta = 1/k_BT$ and α_i are proportionality constants so that eq 3 is recovered (within a constant). In our case, we do not consider ion pairs constrained on the distance but also on an angle. The angle is constrained and not fixed, which means that it fluctuates around the imposed equilibrium value (0° with the normal to the surface; equivalently and for sake of clarity, we show a 90° angle with the surface itself, see Figure 8). With such a geometry, the elementary volume is now $r^2 \sin(\theta)\, \mathrm{d}\theta\mathrm{d}\phi\mathrm{d}r$ so that the probability density distribution is given by

$$\mathcal{P}(r)\mathrm{d}r = \alpha \int \exp\left(-\frac{V^{MM}(r,\theta,\phi) + V(\theta)}{k_BT}\right) r^2 \sin(\theta)\mathrm{d}\theta\mathrm{d}\phi\mathrm{d}r \tag{5}$$

where $V(\theta)$ is the potential energy of the angular constraint. The fluctuations in θ are assumed to be small so that the θ-dependency of the McMillan−Mayer potential $V^{MM}(r,\theta,\phi)$ can be neglected in eq 5. The angular integration can thus be performed independently of r, and the entropic correction (eq 3) is the same as in the case of bulk solutions. Such a correction is mandatory to recover a constant potential at long distances.

2.3. Adjusting the Potential of Mean Force on the Coulomb Term. Umbrella sampling provides the relative free energy as a function of ion separation, where the long-distance separation is typically used as a reference energy state where interfacial effects are negligible. Since the US technique is computationally expensive, only relatively short distances are calculated in this way. This means that a reference state for the PMF has to be chosen independently to reconstruct the whole PMF. This can be done by assuming that the interaction energy beyond a certain distance is dominated by the Coulombic interaction between the ion and the deprotonated oxygen. Therefore, the potential of mean force goes to zero as the Coulombic potential becomes negligible. In this work, the potential of mean force is assumed to be equal to the Coulombic potential at separation distances beyond 1.1 nm.

When considering the electrostatic interaction between two ions, one can simply think of them as point charges. This simplified picture does not hold true for the interaction between an ion and a charged surface, since all surface atoms additively contribute to the electrostatic interaction between the silica and the ion. Only when the ion is sufficiently far from the deprotonated silanol, the total effective Coulombic interaction can be approximated by a punctual charge on the

DOI: 10.1021/acs.jpcc.5b08836
J. Phys. Chem. C 2016, 120, 963−973

deprotonated oxygen. For this reason, beyond 1.1 nm, the PMF is set to be equal to the electrostatic interaction between two punctual charges: the solvated cation and the deprotonated oxygen. In order to calculate the Coulomb energy as a function of distance, we use the dielectric constant for SPC/E water which has been estimated to be 72.4.[37] Regardless of the charge assigned to the surface O_c in the DM model, the long-range part of the bulk PMFis fitted with an oxygen of charge $-1e$, because this charge is the genuine local charge upon deprotonatrion. Consequently, all PMFs are identical at long distances, as can be seen in Figures 4 and 6.

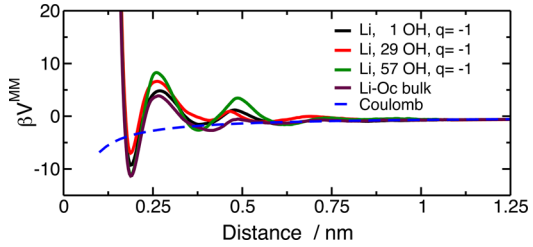

Figure 4. Li−O_c potentials for a $-1e$ charge on oxygen. An activation energy appears for adsorption.

2.4. Reference Bulk Potential of Mean force. In addition to our surface-ion PMFs, we also show the corresponding ion-oxygen PMF profiles in bulk solution for the sake of comparison. For these systems, the oxygen is the bare O_c as described in Table 1. Of course, this bulk O_c is a virtual ion which is only considered for comparison purpose because O^- is not stable in water. It should be mentioned that this virtual O_c is very similar to fluoride ions which have similar Lennard-Jones parameters σ = 3.168 Å and ϵ = 0.836 kJ/mol.[44] Indeed, the PMF for the bulk O_c compares favorably with published results for lithium-fluoride.[48]

3. RESULTS AND DISCUSSION

3.1. Overview of Results. The results for the two ions (Li and Cs) and the two charge sets are shown in Figures 4, 5, 6, and 7. Each figure contains four PMFs, corresponding to the three silanol coverages and the bulk PMF. As expected, increasing the silanol density increases the hydrophilicity of the surface. Each figure includes the Coulomb term which was used to adjust the potentials of mean force at long distances. At short distance, the Coulomb term is limited to typically $-7k_BT$. As mentioned previously, we use the dielectric constant of SPC/E water for the calculation of the Coulomb potential. However, in reality the assumption of a dielectric constant breaks down at a short distance. The used constant will be an overestimation, so that the importance of the Coulomb term in the total PMF is underestimated.

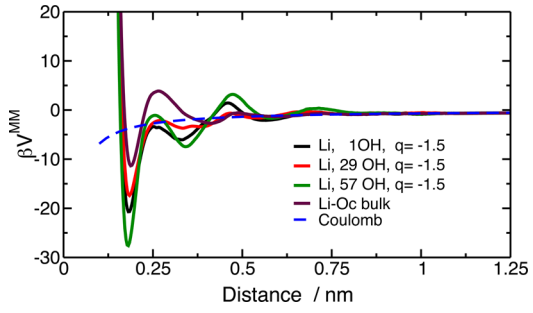

Figure 5. Li−O_c potentials for a $-1.5e$ charge on oxygen. A higher charge on oxygen tends to reduce the activation energy for adsorption.

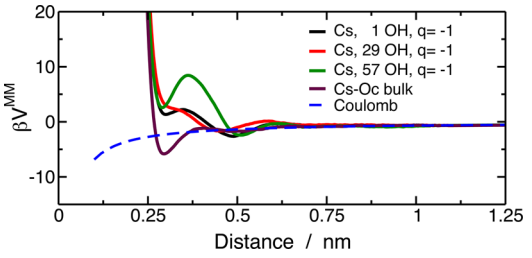

Figure 6. Cs−O_c potentials for a $-1e$ charge on oxygen. Hydrophilicity increases the activation energy for adsorption and desorption of cesium.

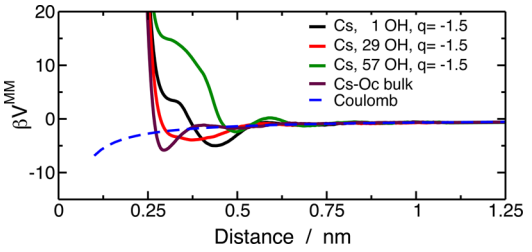

Figure 7. Cs−O_c potentials for a $-1.5e$ charge on oxygen.

We observe a strong attraction in the case of the lithium−oxygen interaction (Figures 4 and 5). Such a contact ion pair (CIP) minimum is close to −15 and −20 kJ/mol for O_c charge equal to −1 or $-1.5e$, respectively. As noted earlier, our results are comparable to LiF interaction as studied by Fennell[48] because the fluoride and the oxygen have similar sizes. These authors showed that a small anion size leads to an increased interaction with small cations. This has important consequences for surfaces that bear charged oxygen atoms, which are likely to form strong bonds with small (or multivalent) cations. On other systems, such as self-assembled monolayers, which show no net charges, PMF profiles are much smoother.[49]

Owing to its larger size, a much smaller attraction is found for cesium compared to lithium (Figures 6 and 7). In contrast to the oxygen−lithium interaction, an increase of the O_c charge tends to repel the cesium ion as a result from the enhanced interaction between the water hydrogen and O_c. The CIP observed for bulk cesium increases for all surfaces typically by 10 kJ/mol for $-1e$ charge and disappears for -1.5 charge.

At intermediate distance (0.5 nm) the PMF oscillates around the Coulomb contribution for the $-1.5e$ charge on oxygen. A similar result is found for solvated ion pairs.[50] It represents the various hydrations of the ion pair (CIP, SSIP, etc.). In contrast, profiles with the charge $-1e$ on the oxygen appear to be less attractive than the reference Coulomb profile at intermediate distance.

3.2. Comparing Ion−Surface to Ion−Ion PMF Profiles. We now compare for each surface the ion−ion and ion−surface PMFs. As already stated, the bulk profile was obtained for a pseudo charged ($-1e$) oxygen atom that is comparable to a fluoride ion. We first consider the case of lithium. For both oxygen charges, we find two minima in the bulk profile, while there are three minima in the ion−surface profiles. The amount of structure formed in the profiles increases with hydrophilicity (Figures 4 and 5) and is stronger near the surface than in the bulk. For cesium, we also observe a difference between the

DOI: 10.1021/acs.jpcc.5b08836
J. Phys. Chem. C 2016, 120, 963−973

profiles corresponding to the bulk profile and those corresponding to surface−ion profiles. We find that the surface is repulsive for cesium; the CIP[51] is clearly seen in the form of the first minimum in the bulk PMFs, while this minimum tends to disappear in the ion−surface PMFs. As discussed above, this effect is more pronounced as the charge on the oxygen increases, due to the increased interaction with the water hydrogen (Figures 6 and 7). The same trend can be observed when changing the surface hydrophilicity. Since cesium ions are larger than lithium ions, the structure of the hydration shells around these larger ions is less pronounced than around smaller ions.[32]

3.3. Dependence of the Ion−Surface PMF on the Constrained Angle θ. We determine the surface−ion interaction with the ion constrained on top of the charged atom. We compare the cases in which the ion is constrained to move only in the direction normal to the surface (90°) or under a 45° angle (Figure 8). There appears to be a difference between the binding energy in both cases (see Figure 9), while the qualitative features in the profiles remain similar.

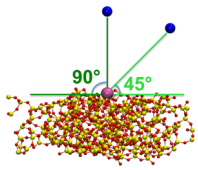

Figure 8. Side view of an ion−surface system, in two cases. The solvated ion can be maintained normal to the surface (90°) directly on top of the charged oxygen site. This is the case in all of our calculations but one. In the latter case, in order to test the influence of the angle on the PMF, the ion is maintained with the angle 45°.

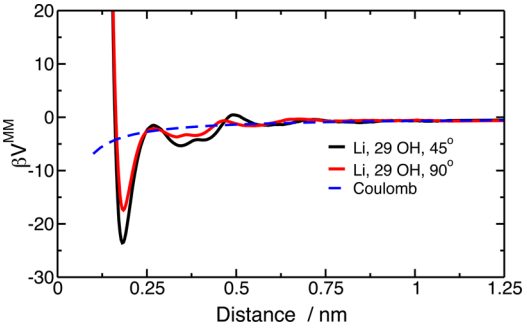

Figure 9. When the Cs−Oxygen−surface angle is reduced from 90° to 45°, the PMF is qualitatively unchanged.

3.4. Effect of Hydrophilicity on Binding. As described earlier, we use three surfaces with different silanol densities in order to discuss the impact of hydrophilicity on the interaction strength. Interestingly, this impact is found to depend on the ion under study. For lithium (Figures 4 and 5), increasing the hydrophilicity significantly deepens the CIP minimum, while for cesium the opposite trend is found (Figures 6 and 7). However, it should be mentioned that the PMFs do not change steadily with the silanol density in the case of the $-1.5e$ charge, indicating that the trend in the data might be a consequence of the ions as well as the site-specific effect; all sites on the surface do not lead to the same PMF profile. A high silanol density reduces the effect of dehydration that occurs upon adsorption, therefore favoring lithium adsorption over cesium adsorption. Assuming that the hydration free energy for lithium is close to $125k_BT$,[51] small differences in this partial dehydration can account for the large energy variation observed in our results for lithium.

3.5. Lithium or Cesium: Which Ion Binds More Strongly? The binding energy of a solvated ion results from the balance of partial dehydration and adsorption energy. It is therefore not straightforward to make a qualitative estimate as to which atom should bind more strongly to a given surface. Figure 10 shows the PMFs for lithium and cesium (on the surface with medium hydrophilicity). It is established that the Gibbs solvation free energy is much larger for lithium than for cesium with a difference that is mostly due to the enthalpy contribution.[51] At first sight, lithium ions bind more strongly than cesium ions, in spite of their higher solvation energy. The radius of lithium is smaller than the radius of cesium, which has a strong impact on energy at contact. When we use a reduced charge on surface sites ($-1e$), the ion surface interaction is reduced, but the impact is stronger on a small ion. The lithium is still the more strongly bonded ion in this case though. These results are in agreement with published results; for example, it is established that Na^+ ions bind more strongly than Cs^+.[7] Binding can be characterized quantitatively with an association constant, as detailed in the next paragraph.

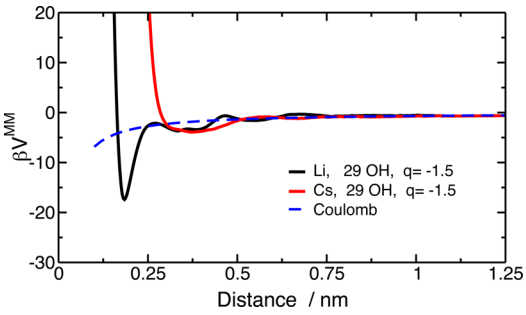

Figure 10. Lithium binding is stronger than cesium binding (profiles repeated from Figure 5 and Figure 7).

3.6. Self-Consistent Concentration Profile. The PMF represents the interaction of a single solvated ion with the surface. For solutions with a large ion concentration, interactions between ions can have an important effect on the adsorption properties and the resulting electric double layer. In order to study this effect, we consider the case with a 0.5 mol L^{-1} ion concentration, where the fluid is confined in a channel of 2 nm wide (Figure 11). This corresponds to five cations in the channel. The ion−ion interaction is assumed to be purely electrostatic. Considering a simple density functional theory (DFT) and the local density approximation (LDA) for ions,[52] the ionic concentration profiles can be calculated by solving self-consistently the following system of equations: Poisson's equation

$$\Delta\psi(z) = -\frac{1}{\epsilon_0\epsilon_r}\rho(z) \tag{6}$$

and Boltzmann's law

$$\rho(z) = \rho_0 \exp\left(-\frac{V^{MM}(z) + e\psi(z)}{k_BT}\right) \tag{7}$$

where V^{MM} is the PMF, ψ the electric potential, ϵ_0 and ϵ_r the vacuum and relative dielectric constant, k_B Boltzmann's constant, T the temperature, and $\rho(z)$ the ion density. We

DOI: 10.1021/acs.jpcc.5b08836
J. Phys. Chem. C 2016, 120, 963−973

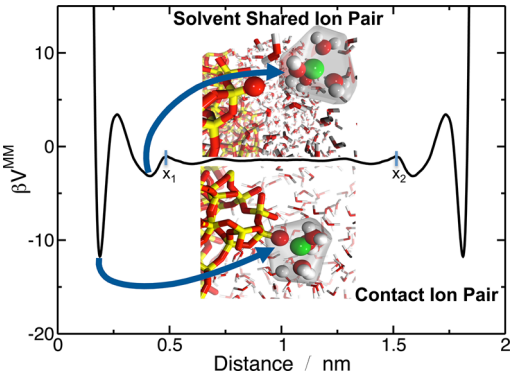

Figure 11. Ion−surface PMF is made symmetrical to produce a model for ion−channel interaction. Silica walls are separated by 2 nm. This distance is between the charged oxygen atom centers.

also have the McMillan−Mayer potential V^{MM}. The potential and its derivative are set to zero in the middle of the channel. In a more realistic model, a three-dimensional (3D) Poisson equation would be coupled with a 3D ion distribution, contrary to eqs 6 and 7, which are one-dimensional (1D) equations. Thus, we have to be cautious with our conclusions. Nevertheless, considering the strong interaction between ions and charged sites, this Boltzmann approximation is probably valid as long as the site is not screened.

Figure 12 shows concentration profiles of the ion solution compared to profiles calculated from the single-ion PMFs.

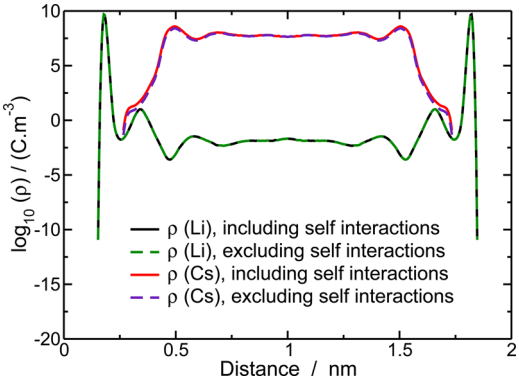

Figure 12. Density profiles at 0.5 mol L^{-1} in a 2 nm wide channel are plotted versus distance. The densities can be estimated with or without self-interaction. The plots refer to 57 OH surfaces and charge −1.5*e*.

Including the self-interaction between the cations solvated in the channel tends to repel ions from the center of the channel. When the ion−surface potential is very attractive, such as for lithium and the oxygen charge −1.5*e*, the two density profiles cannot be distinguished. In the case shown for cesium, the surface is repulsive, and the density increases in the vicinity of walls.

To conclude, considering the geometry, ion−surface interactions appear to be largely dominant. The ion−pair formation appears to be the predominant mechanism in the Stern layer formation. This effect is highly ion specific and also dependent on the details of the interface.

3.7. Association Constants and Mean First Passage Times. *3.7.1. Association Constants.* We consider the association reaction which reads in the case of lithium

$$Li_{aq}^{+} + O_c^{-q} \rightleftharpoons LiO_c^{1-q} \quad (8)$$

$-q$ being the oxygen charge (see Table 2). An association constant can be defined for this reaction. We use a Bjerrum-like association constant[30] to characterize the ion−surface degree of association

$$K_D(d) = \int_0^d dr 2\pi r^2 e^{-\beta V^{MM}(r)} \quad (9)$$

The association constant depends on d, the chosen limit to distinguish associated from dissociated pairs. We choose the second maximum of the potentials, namely 0.5 and 0.6 nm, for lithium and cesium, respectively (see x_1 and x_2 in Figure 11). These positions correspond to the first local maximum beyond the SSIP. We use 2π instead of 4π in the association constant formula (eq 9) because only half of the space is available for the solvent. When ion−ion interactions are estimated, the interaction potentials are spherically symmetrical, which is not the case for ion−surface interactions. Our results above show that the sensitivity of the PMF to the ion−surface angle is relatively small so that the association constant can be determined from the PMF along the surface normal.

Table 3 shows the calculated association constants. For the smaller charge on the deprotonated oxygen, the adsorption

Table 3. Association Constants (K_D in L mol^{-1}, with Natural Logarithm ln) and Mean First Passage Time (MFPT, in s) for Lithium and Cesium, Two Effective Charges on Deprotonated Oxygen and Three Numbers of Silanols per 2.852² nm^2[a]

ion	charge	silanols	ln(K_D)	τ_{ads}	τ_{des}
		1	3.0	1.8×10^{-10}	7.7×10^{-7}
Li	−1.0	29	0.6	1.4×10^{-10}	4.1×10^{-7}
		57	4.7	5.4×10^{-10}	9.4×10^{-5}
		1	0.11	4.9×10^{-11}	1.9×10^{-11}
Cs	−1.0	29	−0.74	5.1×10^{-11}	2.5×10^{-11}
		57	−0.21	5.3×10^{-11}	1.0×10^{-11}
		1	14	1.2×10^{-10}	1.9×10^{-3}
Li	−1.5	29	11	1.1×10^{-10}	1.5×10^{-5}
		57	21	2.5×10^{-10}	7.7
		1	2.0	3.9×10^{-11}	1.7×10^{-10}
Cs	−1.5	29	1.2	4.0×10^{-11}	1.2×10^{-10}
		57	−0.45	4.6×10^{-11}	2.0×10^{-11}
Li	−1.0	bulk	5.0	1.3×10^{-10}	2.1×10^{-6}
Cs	−1.0	bulk	1.4	4.1×10^{-11}	3.5×10^{-10}

[a]Boundaries for mean residence times are illustrated in Figure 11. MFPT center is the average time needed for an ion in the middle of the slit pore at the initial time to go beyond x_1 or x_2. MFPT bonded is the average time needed for a bonded ion on the right side, to go beyond x_1. Values obtained with ion−ion potentials are indicated with "bulk".

constant is a lower limit to the real value. When comparing results for different effective charges, we conclude that the association constant is very sensitive to the charge. The association constants in Table 2 confirm the intuition from the PMFs: lithium binds more strongly than cesium, and hydrophilicity increases lithium adsorption and reduces cesium adsorption.

3.7.2. Mean First Passage Times. When an external field is applied to the system, the motion of ions is the cumulative result of streaming and diffusion (caused by thermal motion).

DOI: 10.1021/acs.jpcc.5b08836
J. Phys. Chem. C 2016, 120, 963−973

The association constant that has been introduced above is a static parameter, not sufficient to predict binding times under the influence of an external field. Instead we use the mean first passage time (MFPT), which is a dynamical quantity related to the average time needed for a particle submitted to an external field to leave a determined region.[18,53] We calculate the MFPT for an absorbing ion in a 2 nm wide channel. Close to the interface, the surface exerts a force on the ion, which is the gradient of the (symmetrical) PMF shown in Figure 11. We consider a cation having a self-diffusion coefficient D subject to an external potential U.[54] If we consider an ion, starting from a position x, the average time needed to go beyond the absorbing boundaries x_1 or x_2, namely, to adsorb on the surface, τ_{ads} reads[18,53]

$$\tau_{ads}(x) = \int_x^{x_2} dq e^{U(q)/k_BT}\left[\left(\frac{1}{D}\int_{x_1}^{q} e^{-U(s)/k_BT} ds\right) - \left(\frac{1}{I}\int_{x_1}^{x_2} dr e^{U(r)/k_BT}\left(\frac{1}{D}\int_{x_1}^{r} e^{U(s)/k_BT} ds\right)\right)\right] \quad (10)$$

with

$$I = \int_{x_1}^{x_2} dq e^{U(q)/k_BT} \quad (11)$$

The average residence time of the ion within the boundaries (i.e., the time it takes the ion to reach the boundaries) is the mean first passage time. In the following, we present MFPT values for x = 1 nm, with x_1 and x_2 as shown in Figure 11. We consider also the case in which a boundary is reflective and the other absorbing: the silica wall is reflective, and x_1 is absorbing. It leads to the desorption MFPT τ_{des} given by[18,53]

$$\tau_{des}(x) = \frac{1}{D}\int_x^{x_1} dq e^{U(q)/k_BT}\int_{wall}^{q} ds e^{-U(s)/k_BT} \quad (12)$$

We present in the following MFPT values for x equal to CIP distance and x_1 as shown in Figure 11

Two series of results are presented: one considering an ion at the pore center, the absorbing boundaries being the second maximum, as detailed for the association constants. The MFPT is in this case the average time needed for a free ion to adsorb on the surface. We present also the case of a bonded ion, i.e., an ion located at the minimum of PMF. In this case, one boundary is reflecting and the other is absorbing. The MFPT is the average time needed for a bonded atom to desorb from the surface. All MFPT values are shown in Table 3.

In order to accumulate a representative phase-space sample, a molecular dynamics simulation should last at least 10 times the duration of the slowest event it includes, being the desorption time for the systems studied here. If we consider that a tractable run lasts 100 ns, we conclude that modeling an equilibrium state for lithium adsorption is not feasible when τ_{des} is above 10^{-9} s. When we consider the time needed for an ion to go from the channel center to beyond the x_1 or x_2 positions (Figure 11), the approximation of a constant diffusion coefficient for the ions, close to its bulk value, is correct. In contrast, when we consider the time needed for an ion to leave from the CIP position, the ion bulk diffusion coefficient we use is an overestimation since the local diffusion coefficient is reduced close to the interface. Molecular dynamics results indicate that the diffusion coefficient of water can be reduced by a factor of 2 in the vicinity of surfaces.[18] The overestimated diffusion means that the calculated MFPT is a lower limit value and that the actual value might be higher.

The existence of an activation barrier not only for unbinding but also for binding should be mentioned. Depending on their magnitude, these barriers indicate that MD simulations can show an out-of-equilibrium population of ions. This can be stated more quantitatively. We consider the case of lithium with 57 OH and O_c charge equal to −1.5. In this case, the average time needed for an ion at the center of the channel to bind to the surface is 0.24 ns. This means that simulations of lithium at silica surfaces can result in out-of-equilibrium concentration profiles unless the simulations are at least 2.4 ns long.

The situation is even worse for desorption for which the characteristic times can be more than 1 s. In that case, the desorption/adsorption equilibria can never be simulated with molecular dynamics since adsorbed ions cannot practically leave their sites.

These binding times predominantly affect the Stern layer: the ions have a higher mobility when they are in SSIP position or more distant to the surface charge. An out-of-equilibrium situation would especially impact electrokinetic predictions that would be deduced from ion concentration profiles.

3.8. Comparison with Experiment. *3.8.1. Comparing Binding of Lithium and Cesium.* A few theoretical studies can be mentioned, which indicate that, along the alkali series, binding on a charged silica oxygen is stronger for the smaller ion. This is the case for Dewan[7] who compares sodium and cesium, Hartkamp et al.[15] who compare sodium and cesium, and Kroutil et al.[55] who compare sodium and rubidium. According to our models, lithium binding is stronger that cesium binding. Are these results confirmed by experiments? Chapel et al.[56] perform force measurements between pyrogenic silica sheets. When a negative surface binds with cations, it creates a surface dipole, made of the surface charge and the diffuse layer. When two similar surfaces are faced, their dipoles interact repulsively. This is the long-range part of the DLVO model[57,58] (Derjaguin−Landau−Verwey−Overbeek). When the surface charge is reduced, for example with stronger ion binding, the dipole diminishes, along with the magnitude of the ζ potential, and this reduces the long-range repulsive force. When comparing in Figure 2 of Chapel et al.,[56] the long-range force is smaller for LiCl than for CsCl, which can be interpreted as a stronger binding for lithium. Although this conclusion is not universal, Franks et al.[59] state that "Most investigations find the absorption sequence···($Cs^+ > K^+ > Na^+ > Li^+$)." This paper is cited by Morag et al. in a recent publication.[60] Morag analyzes the Hofmeister alkali series reversal with pH on silica. He states that at low pH the preferential adsorption of cesium is not driven by electrostatics but by the weak hydration of this big cation. A crossover takes place around pH = 6. For pH above this limit, more silanol are deprotonated, favoring lithium adsorption. Indeed, our model concerns the high pH limit since we consider deprotonated silanols. We can state that, on this debated topic, our model tends to confirm the recent conclusions of Morag.

3.8.2. Is Cesium Repulsion Corroborated by Experiment ? If we consider Figure 6 and Figure 7, we see that cesium surface interaction can be repulsive on a large domain. This is particularly true for the first PMF minimum at 0.3 nm. Consistently, association constants in Table 3 for cesium are quite small, although they include association not only for CIP at 0.3 nm but also for SSIP at 0.45 nm. This repulsion is a typical surface effect since it does not appear for the reference

DOI: 10.1021/acs.jpcc.5b08836
J. Phys. Chem. C 2016, 120, 963−973

bulk PMF, plotted on the same figures. An intriguing point is that increasing the negative charge has a strong effect on lithium but much smaller on cesium. Morag et al.[60] mention the popular assumption that cation adsorption is invariably driven by electrostactics. If it were the case for cesium, the $-1.5e$ on oxygen would produce a higher adsorption. Morag states that hydrogen bonds of charged silanol with water suppress cesium adsorption. In other words, the competition of water and cesium for binding to surface oxygen is in favor of water. Our results tend to confirm this point of view. At low pH, the silica surfaces show fewer silanol, and cesium adsorption can occur on neutral sites rather than on charged sites, which, paradoxally, tend to repel these cations.[60] Since we model a charged deprotonated silanol, we model in the limit of high pH solution, for which cesium tends to be repelled by the surface.

4. CONCLUSION

We have performed molecular dynamics simulations of charged amorphous silica surfaces in contact with water and cations, for increasing surface hydrophilicity. The McMillan−Mayer PMF is found to exhibit strong ion specificity with qualitatively different trends for lithium and cesium. Lithium binds more strongly than cesium due to their smaller size, and their adsorption is favored by hydrophilicity, in contrast to cesium. Lithium binding is strong, while cesium is repelled by the surface. These results are confirmed by recent experiment in the limit of high pH. Our results show that the diffuse layer is larger for cesium than for lithium. It must be noted though that only a single adsorption site is studied. The amount and density of charge sites are also important for the adsorption properties. It is likely that only one PMF is not enough to characterize the ion/surface interaction: a distribution of PMF that could represent the site polydispersity would be desirable. Regardless, the ion−surface PMFs are not very different from the one in bulk solutions, and the familiar concepts of Bjerrum association, CIP, or SSIP can still be applied.

Our analysis provides a new image of the Stern layer. Generally speaking, the Stern layer is not a continuous layer but a set of attracting points giving rise to contact ion pairs. These points are not equivalent from the adsorption point of view. Within this context, condensation is specific both for the ions and the surface since local variations of proton surface density impact it.

The primary interest of the McMillan−Mayer ion−surface PMF is the fact that it can be used for macroscopic modeling, by generalizing the original Gouy−Chapman theory based on the Poisson−Boltzmann equation. In fact we have to be cautious with mesoscopic modeling. Most of such approaches actually use 1D models (as the DFT calculation we performed in this article). Nevertheless, the Stern layer appears to be in fact a collection of localized charges inhomogeneously distributed near the sites at the silica surface. The global potential of mean force between the surface is the sum of all the site contributions. If a macroscopic continuous solvent model is to be produced, it would probably be necessary to include three dimensions because CIP requires such anisotropic modeling. All 1D models of charged interfaces, even when based on molecular results, are actually *effective* models that cannot take proper account of the Stern layer.

The adsorption times calculated here illustrate that relaxation of a system involving ions at charged surfaces can be slow compared to the simulation time of a typical molecular dynamics simulation. This is especially likely to be the case for multivalent ions. The adsorption mechanism is globally similar to the one of ion binding in bulk water. There is a global trend to higher activation energy upon binding in the case of surface adsorption. An important consequence of this work is the fact that all molecular models, including highly binding ions facing charged surfaces, should be considered with caution. The activation energy can be relatively high, and it can take a very long time (up to the order of seconds even for simple monovalent ions) to equilibrate the system. Because of the time limitation of simulations, it is likely that molecular dynamics models sometimes produce out-of-equilibrium concentration profiles which, in turn, greatly affect electrodynamics analysis.

AUTHOR INFORMATION

Corresponding Authors

*E-mail: bertrand.siboulet@cea.fr

*E-mail: jean-francois.dufreche@icsm.fr.

Notes

The authors declare no competing financial interest.

ACKNOWLEDGMENTS

The authors are particularly grateful to Thomas Zemb for fruitful discussions. This research was partially supported by the program NEEDS (Projet fédérateur milieux poreux : MIPOR).

REFERENCES

(1) Lyklema, J. *Solid-Liquid Interfaces*; Fundamentals of interface and Colloid Science; Academic Press: Amsterdam, 2005; Vol. 2.

(2) Attard, P.; Antelmi, D.; Larson, I. Comparison of the Zeta Potential with the Diffuse Layer Potential from Charge Titration. *Langmuir* **2000**, *16*, 1542−1552.

(3) Larson, I.; Attard, P. Surface Charge of Silver Iodide and Several Metal Oxides. Are All Surfaces Nernstian? *J. Colloid Interface Sci.* **2000**, *227*, 152−163.

(4) Dufreche, J.-F.; Marry, V.; Bernard, O.; Turq, P. Models for Electrokinetic Phenomena in Montmorillonite. *Colloids Surf., A* **2001**, *195*, 171−180.

(5) Dufreche, J.-F.; Marry, V.; Malikova, N.; Turq, P. Molecular Hydrodynamics for Electro-Osmosis in Clays: from Kubo to Smoluchowski. *J. Mol. Liq.* **2005**, *118*, 145−153.

(6) Marry, V.; Dufreche, J.-F.; Jardat, M.; Turq, P. Equilibrium and Electrokinetic Phenomena in Charged Porous Media from Microscopic and Mesoscopic Models: Electro-Osmosis in Montmorillonite. *Mol. Phys.* **2003**, *101*, 3111−3119.

(7) Dewan, S.; Carnevale, V.; Bankura, A.; Eftekhari-Bafrooei, A.; Fiorin, G.; Klein, M. L.; Borguet, E. Structure of Water at Charged Interfaces: A Molecular Dynamics Study. *Langmuir* **2014**, *30*, 8056−8065.

(8) Cazade, P.-A.; Hartkamp, R.; Coasne, B. Structure and Dynamics of an Electrolyte Confined in Charged Nanopores. *J. Phys. Chem. C* **2014**, *118*, 5061−5072.

(9) Bocquet, L.; Charlaix, E. Nanofluidics, from Bulk to Interfaces. *Chem. Soc. Rev.* **2009**, *39*, 1073−1095.

(10) Renou, R.; Szymczyk, A.; Ghoufi, A. Ultraconfinement of aqueous electrolytic solutions within hydrophilic nanotubes. *RSC Adv.* **2014**, *4*, 32755−32761.

(11) Renou, R.; Ghoufi, A.; Szymczyk, A.; Zhu, H.; Neyt, J. C.; Malfreyt, P. Nanoconfined Electrolyte Solutions in Porous Hydrophilic Silica Membranes. *J. Phys. Chem. C* **2013**, *117*, 11017−11027.

(12) Rizzi, F.; Jones, R. E.; Debusschere, B. J.; Knio, O. M. Uncertainty Quantification in MD Simulations of Concentration Driven Ionic Flow through a Silica Nanopore. I. Sensitivity to Physical Parameters of the Pore. *J. Chem. Phys.* **2013**, *138*, 194104.

(13) Ho, T. A.; Argyris, D.; Cole, D. R.; Striolo, A. Aqueous NaCl and CsCl Solutions Confined in Crystalline Slit-Shaped Silica

DOI: 10.1021/acs.jpcc.5b08836
J. Phys. Chem. C 2016, 120, 963−973

Nanopores of Varying Degree of Protonation. *Langmuir* **2011**, *28*, 1256−1266.
(14) Zhu, H.; Ghoufi, A.; Szymczyk, A.; Balannec, B.; Morineau, D. Computation of the Hindrance Factor for the Diffusion for Nanoconfined Ions: Molecular Dynamics Simulations versus Continuum-Based Models. *Mol. Phys.* **2012**, *110*, 1107−1114.
(15) Hartkamp, R.; Siboulet, B.; Dufreche, J.-F.; Coasne, B. Ion-Specific Adsorption and Electroosmosis in Charged Amorphous Porous Silica. *Phys. Chem. Chem. Phys.* **2015**, *17*, 24683−24695.
(16) Zhuravlev, L. Concentration of Hydroxyl-Groups on the Surface of Amorphous Silicas. *Langmuir* **1987**, *3*, 316−318.
(17) Karlsson, M.; Craven, C.; Dove, P. M.; Casey, W. H. Surface Charge Concentrations on Silica in Different 1.0 m Metal-Chloride Background Electrolytes and Implications for Dissolution Rates. *Aquat. Geochem.* **2001**, *7*, 13−32.
(18) Siboulet, B.; Molina, J.; Turq, P.; Dufreche, J.-F. Water Self-Diffusion at the Surface of Silica Glasses: Effect of Hydrophobic to Hydrophilic Transition. *Mol. Phys.* **2013**, *111*, 3410−3417.
(19) Siboulet, B.; Coasne, B.; Dufreche, J.-F.; Turq, P. Hydrophobic Transition in Porous Amorphous Silica. *J. Phys. Chem. B* **2011**, *115*, 7881−7886.
(20) Markesteijn, A. P.; Hartkamp, R.; Luding, S.; Westerweel, J. A Comparison of the Value of Viscosity for Several Water Models Using Poiseuille Flow in a Nano-channel. *J. Chem. Phys.* **2012**, *136*, 134104.
(21) Haria, N. R.; Lorenz, C. D. Ion Exclusion and Electrokinetic Effects Resulting from Electro-Osmotic Flow of Salt Solutions in Charged Silica Nanopores. *Phys. Chem. Chem. Phys.* **2012**, *14*, 5935−5944.
(22) Lorenz, C. D.; Crozier, P. S.; Anderson, J. A.; Travesset, A. Molecular Dynamics of Ionic Transport and Electrokinetic Effects in Realistic Silica Channels. *J. Phys. Chem. C* **2008**, *112*, 10222−10232.
(23) Cruz-Chu, E.; Aksimentiev, A.; Schulten, K. Water-Silica Force Field for Simulating Nanodevices. *J. Phys. Chem. B* **2006**, *110*, 21497−21508.
(24) Zhang, H.; Hassanali, A. A.; Shin, Y. K.; Knight, C.; Singer, S. J. The Water-Amorphous Silica Interface: Analysis of the Stern Layer and Surface Conduction. *J. Chem. Phys.* **2011**, *134*, 024705.
(25) Haria, N. R.; Lorenz, C. D. Atomistic Description of Pressure-Driven Flow of Aqueous Salt Solutions through Charged Silica Nanopores. *J. Phys. Chem. C* **2015**, *119*, 12298−12311.
(26) McMillan, W. G.; Mayer, J. E. The Statistical Thermodynamics of Multicomponent Systems. *J. Chem. Phys.* **1945**, *13*, 276−305.
(27) Friedman, H. L. *A Course in Statistical Mechanics*; Prentice-Hall: Englewood Cliffs, New Jersey, 07632, 1985.
(28) Lyubartsev, A. P.; Marcelja, S. Evaluation of Effective Ion-Ion Potentials in Aqueous Electrolytes. *Phys. Rev. E: Stat. Phys., Plasmas, Fluids, Relat. Interdiscip. Top.* **2002**, *65*, 041202.
(29) Molina, J. J.; Dufreche, J.-F.; Salanne, M.; Bernard, O.; Jardat, M.; Turq, P. Models of Electrolyte Solutions from Molecular Descriptions: The Example of NaCl Solutions. *Phys. Rev. E* **2009**, *80*, 065103.
(30) Molina, J. J.; Dufreche, J.-F.; Salanne, M.; Bernard, O.; Turq, P. Primitive Models of Ions in Solution from Molecular Descriptions: A Perturbation Approach. *J. Chem. Phys.* **2011**, *135*, 234509.
(31) Nguyen, T.-N.; Duvail, M.; Villard, A.; Molina, J. J.; Guilbaud, P.; Dufreche, J.-F. Multi-Scale Modelling of Uranyl Chloride Solutions. *J. Chem. Phys.* **2015**, *142*, 024501.
(32) Hartkamp, R.; Coasne, B. Structure and Transport of Aqueous Electrolytes: From Simple Halides to Radionuclide Ions. *J. Chem. Phys.* **2014**, *141*, 124508.
(33) Bonnaud, P.; Coasne, B.; Pellenq, R. Molecular Simulation of Water Confined in Nanoporous Silica. *J. Phys.: Condens. Matter* **2010**, *22*, 284110−284124.
(34) Puibasset, J.; Pellenq, R. Grand Canonical Monte Carlo Simulation Study of Water Structure on Hydrophilic Mesoporous and Plane Silica Substrates. *J. Chem. Phys.* **2003**, *119*, 9226−9232.
(35) Berendsen, H.; Grigera, J.; Straatsma, T. The Missing Term in Effective Pair Potentials. *J. Phys. Chem.* **1987**, *91*, 6269−6271.
(36) Berendsen, H.; Postma, J.; Vangunsteren, W.; Dinola, A.; Haak, J. Molecular-Dynamics with Coupling to an External Bath. *J. Chem. Phys.* **1984**, *81*, 3684−3690.
(37) Gereben, O.; Pusztai, L. On the Accurate Calculation of the Dielectric Constant from Molecular Dynamics Simulations: The Case of SPC/E and SWM4-DP Water. *Chem. Phys. Lett.* **2011**, *507*, 80−83.
(38) Todorov, I. T.; Smith, W.; Trachenko, K.; Dove, M. T. DL_POLY_3: New Dimensions in Molecular Dynamics Simulations via Massive Parallelism. *J. Mater. Chem.* **2006**, *16*, 1911−1918.
(39) Grossfield, A. WHAM: An Implementation of the Weighted Histogram Analysis Method. http://membrane.urmc.rochester.edu/content/wham, Version 2.0.9, accessed on 2015/03/01.
(40) Wolfram Research Inc., Mathematica. Mathematica Version 8.0.
(41) Humphrey, W.; Dalke, A.; Schulten, K. VMD: Visual Molecular Dynamics. *J. Mol. Graphics* **1996**, *14*, 33−38.
(42) Rasaiah, J.; Lynden-Bell, R. Computer Simulation Studies of the Structure and Dynamics of Ions and Non-Polar Solutes in Water. *Philos. Trans. R. Soc., A* **2001**, *359*, 1545−1574.
(43) Lee, S.; Rossky, P. A Comparison of the Structure and Dynamics of Liquid Water at Hydrophobic and Hydrophilic Surfaces - a Molecular-Dynamics Simulation Study. *J. Chem. Phys.* **1994**, *100*, 3334−3345.
(44) Dang, L. X. Development of Nonadditive Intermolecular Potentials Using Molecular-Dynamics - Solvation of Li+ and F- Ions in Polarizable Water. *J. Chem. Phys.* **1992**, *96*, 6970−6977.
(45) Kumar, S.; Rosenberg, J. M.; Bouzida, D.; Swendsen, R. H.; Kollman, P. A. The Weighted Histogram Analysis Method for Free-Energy Calculations on Biomolecules. I. The Method. *J. Comput. Chem.* **1992**, *13*, 1011−1021.
(46) Kumar, S.; Rosenberg, J. M.; Bouzida, D.; Swendsen, R. H.; Kollman, P. A. Multidimensional Free-Energy Calculations Using the Weighted Histogram Analysis Method. *J. Comput. Chem.* **1995**, *16*, 1339−1350.
(47) Souaille, M.; Roux, B. Extension to the Weighted Histogram Analysis Method: Combining Umbrella Sampling with Free Energy Calculations. *Comput. Phys. Commun.* **2001**, *135*, 40−57.
(48) Fennell, C. J.; Bizjak, A.; Vlachy, V.; Dill, K. A. Ion Pairing in Molecular Simulations of Aqueous Alkali Halide Solutions. *J. Phys. Chem. B* **2009**, *113*, 6782−6791.
(49) Schwierz, N.; Horinek, D.; Netz, R. R. Anionic and Cationic Hofmeister Effects on Hydrophobic and Hydrophilic Surfaces. *Langmuir* **2013**, *29*, 2602−2614.
(50) Molina, J. J.; Duvail, M.; Dufreche, J.-F.; Guilbaud, P. Atomistic Description of Binary Lanthanoid Salt Solutions: A Coarse-Graining Approach. *J. Phys. Chem. B* **2011**, *115*, 4329−4340.
(51) Marcus, Y. *Ion solvation*; John Wiley and Sons Ltd.: Chichester, 1985.
(52) *Fundamentals of Inhomogeneous Fluids*; Marcel Dekker, Inc: New York, 1992.
(53) Zwanzig, R. *Nonequilibrium Statistical Mechanics*; Oxford University Press USA: New York, 2001.
(54) Braun, B. M.; Weingaertner, H. Accurate Self-Diffusion Coefficients of Lithium(1+), Sodium(1+), and Cesium(1+) Ions in Aqueous Alkali Metal Halide Solutions from NMR Spin-Echo Experiments. *J. Phys. Chem.* **1988**, *92*, 1342−1346.
(55) Kroutil, O.; Chval, Z.; Skelton, A. A.; Předota, M. Computer Simulations of Quartz (101)-Water Interface over a Range of pH Values. *J. Phys. Chem. C* **2015**, *119*, 9274−9286.
(56) Chapel, J. Electrolyte Species-Dependent Hydration Forces between Silica Surfaces. *Langmuir* **1994**, *10*, 4237−4243.
(57) Derjaguin, B.; Landau, L. Theory of the Stability of Strongly Charged Lyophobic Sols and of the Adhesion of Strongly Charged Particles in Solutions of Electrolytes. *Acta Phys. Chem.* **1941**, *14*, 633−662.
(58) Verwey, E. J. W.; Overbeek, J. T. G. In *Theory of the stability of lyophobic colloids*; Verwey, E. J. W., Overbeek, J. T. G., Eds.; Elsevier: Amsterdam, 1948.
(59) Franks, G. Zeta Potentials and Yield Stresses of Silica Suspensions in Concentrated Monovalent Electrolytes: Isoelectric

DOI: 10.1021/acs.jpcc.5b08836
J. Phys. Chem. C 2016, 120, 963−973

Point Shift and Additional Attraction. *J. Colloid Interface Sci.* **2002**, *249*, 44−51.
(60) Morag, J.; Dishon, M.; Sivan, U. The Governing Role of Surface Hydration in Ion Specific Adsorption to Silica: An AFM-Based Account of the Hofmeister Universality and Its Reversal. *Langmuir* **2013**, *29*, 6317−6322.

■ NOTE ADDED AFTER ASAP PUBLICATION

This paper was published to the Web on January 4, 2016, with an error in Table 2. This was corrected in the version published to the Web on January 7, 2016.

DOI: 10.1021/acs.jpcc.5b08836
J. Phys. Chem. C 2016, 120, 963−973